



Cite this: *RSC Adv.*, 2024, **14**, 15413

## Ultrasmall copper nanoclusters as an efficient antibacterial agent for primary peritonitis therapy†

Yaru Wang,<sup>a</sup> Jingrun Ye,<sup>b</sup> Kang Liu,<sup>\*a</sup> Yinghao Wu,<sup>a</sup> Jiayi Linghu,<sup>a</sup> Ting Feng,<sup>a</sup> Yong Liu,<sup>ID</sup><sup>a</sup> Xinyue Dou,<sup>a</sup> Xun Yuan,<sup>ID</sup><sup>\*a</sup> and Haiguang Zhu,<sup>ID</sup><sup>\*a</sup>

The urgent need to develop biocompatible, non-resistant antibacterial agents to effectively combat Gram-negative bacterial infections, particularly for the treatment of peritonitis, presents a significant challenge. In this study, we introduce our water-soluble Cu<sub>30</sub> nanoclusters (NCs) as a potent and versatile antibacterial agent tailored for addressing peritonitis. The as-synthesized atomically precise Cu<sub>30</sub> NCs demonstrate exceptional broad-spectrum antibacterial performance, and especially outstanding bactericidal activity of 100% against Gram-negative *Escherichia coli* (*E. coli*). Our *in vivo* experimental findings indicate that the Cu<sub>30</sub> NCs exhibit remarkable therapeutic efficacy against primary peritonitis caused by *E. coli* infection. Specifically, the treatment leads to a profound reduction of drug-resistant bacteria in the peritoneal cavity of mice with peritonitis by more than 5 orders of magnitude, along with the resolution of pathological features in the peritoneum and spleen. Additionally, comprehensive *in vivo* biosafety assessment underscores the remarkable biocompatibility, low biotoxicity, as well as efficient hepatic and renal clearance of Cu<sub>30</sub> NCs, emphasizing their potential for *in vivo* application. This investigation is poised to advance the development of novel Cu NC-based antibacterial agents for *in vivo* antibacterial treatment and the elimination of abdominal inflammation.

Received 8th March 2024  
 Accepted 27th April 2024

DOI: 10.1039/d4ra01785d  
[rsc.li/rsc-advances](http://rsc.li/rsc-advances)

### 1. Introduction

Bacterial infections pose a significant threat to global public health and human well-being, with approximately 700 000 people succumbing to drug-resistant bacterial infections annually, according to the World Health Organization.<sup>1</sup> Although antibiotics have historically been effective in combating bacterial infections, the widespread overuse and abuse of these drugs have escalated the issue of bacterial resistance.<sup>2–5</sup> Notably, different from the situation that Gram-positive bacteria could be easily treated by novel drugs targeting Gram-positive bacteria in clinical trials, the unique structure of Gram-negative bacteria, and their proclivity for transmitting drug resistance have significantly impeded the development of new antibiotics targeting these bacteria over the last two decades.<sup>6,7</sup> This has rendered the treatment of Gram-negative infections particularly challenging.<sup>4,8</sup> Gram-negative bacterial infections can be classified into local and systemic infections according to the different infection sites. Local infections are typically confined to the skin or organs, while

systemic infections are commonly associated with abdominal cavity or bloodstream infections. Among these infections, primary peritonitis, a serious systemic infection caused by Gram-negative bacteria in the abdominal cavity, merits particular attention. Without timely treatment, peritonitis can precipitate systemic multiple organ failure, septic shock, and death.<sup>9–11</sup> Therefore, the pressing need to develop new, non-resistant antibacterial agents to combat Gram-negative bacterial infections, notably to effectively manage peritonitis, cannot be overstated.<sup>12</sup>

In recent years, there has been a surge in the development of ultrasmall coinage metal nanoclusters (NCs; *e.g.*, Au and Ag) with a core size of <3 nm,<sup>13–15</sup> which have gained widespread acceptance in various biomedical applications such as bio-imaging,<sup>16,17</sup> drug delivery,<sup>18</sup> disease theranostic,<sup>19</sup> and broad-spectrum antibacterial.<sup>1</sup> Metal NCs exhibit atomically precise size,<sup>20,21</sup> molecule-like luminescence,<sup>22–26</sup> good biocompatibility,<sup>27</sup> size/structure-dependent physicochemical properties,<sup>28–30</sup> strong antibacterial activity,<sup>31,32</sup> and no drug resistance,<sup>1</sup> rendering them effective in diverse antibacterial applications.<sup>1,19,31,33</sup> Notably, a series of Au and Ag NCs-based antibacterials have demonstrated either long-lasting photodynamic antibacterial performance or intrinsic antibacterial activity,<sup>31,32</sup> thereby promoting the healing of bacteria-infected wounds.<sup>34,35</sup> However, previous studies on metal NCs-based antibacterials have predominantly focused on the treatment of local infections, neglecting systemic ones. Moreover, the

<sup>a</sup>School of Materials Science and Engineering, Qingdao University of Science and Technology, Qingdao 266042, PR China. E-mail: [yuanxun@qust.edu.cn](mailto:yuanxun@qust.edu.cn); [zhuhg@qust.edu.cn](mailto:zhuhg@qust.edu.cn)

<sup>b</sup>School of Chemistry and Molecular Engineering, Qingdao University of Science and Technology, Qingdao 266042, PR China

† Electronic supplementary information (ESI) available. See DOI: <https://doi.org/10.1039/d4ra01785d>



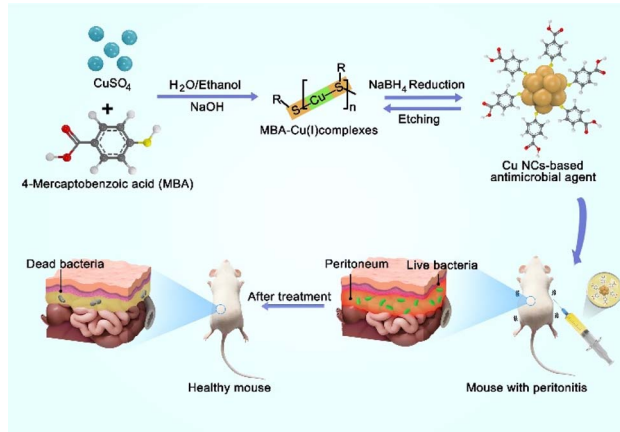
limited availability of Au and Ag on Earth hinders their widespread utilization in cost-effective antibacterial applications. Conversely, copper (Cu), belonging to the same IB group as Au and Ag and being abundant, presents a promising alternative for developing affordable yet efficient metal NCs-based antibacterial agents.<sup>33,36</sup> Nevertheless, the easy oxidation of Cu and the infeasibility of previously used synthetic strategies for Au and Ag NCs pose challenges in the synthesis of atomically precise water-soluble Cu NCs. Consequently, the development of low-cost water-soluble Cu NCs-based antibacterial agents and their application to systemic infections, such as peritonitis caused by Gram-negative bacteria, hold considerable potential for research and clinical value, thereby motivating this project.

In this study, we present our design of water-soluble Cu<sub>30</sub> NCs as a potent and versatile antibacterial agent for the effective treatment of peritonitis (Scheme 1). The synthesized Cu<sub>30</sub> NCs exhibit a monodisperse size at the atomic level, and have demonstrated outstanding broad-spectrum antibacterial activity. They have been shown to achieve bactericidal rates of more than 99% against both Gram-negative *Escherichia coli* (*E. coli*), Gram-positive *Staphylococcus aureus* (*S. aureus*), and the fungus *Candida albicans*, and >97% against obstinate methicillin-resistant *S. aureus* (MRSA). Moreover, the *in vivo* evaluation of Cu<sub>30</sub> NCs, administered through intraperitoneal injection, against primary peritonitis caused by Gram-negative *E. coli* has shown their efficacy for peritonitis treatment and reducing inflammation in bacterial infections. Furthermore, both *in vitro* and *in vivo* studies have revealed the good biocompatibility of the Cu<sub>30</sub> NCs, emphasizing their suitability for combatting systemic infections. To the best of our knowledge, this study represents the first successful application of ultrasmall Cu NCs-based antibacterial agents in the treatment of primary peritonitis.

## 2. Result and discussion

### 2.1 Synthesis and characterization of Cu<sub>30</sub> NCs

The synthesis of Cu<sub>30</sub> NCs in this study was accomplished using the previously reported “NaOH-mediated NaBH<sub>4</sub> reduction”



**Scheme 1** Schematic illustration of the synthesis of Cu<sub>30</sub> NCs and their antibacterial application in treating primary peritonitis.

method. It should be mentioned that optimal pH and solvent polarity are the key parameters to obtain monodisperse Cu<sub>30</sub> NCs. Specifically, NaOH was found to modulate the reduction ability of NaBH<sub>4</sub> by impeding its self-hydrolysis, while concurrently heightening the etching ability of thiolate ligands by deprotonating free ligands in an alkaline environment. Additionally, the mixed water/ethanol solvent was instrumental in fine-tuning the size and structure of MBA-Cu(I) complexes. Therefore, the absence of NaOH and ethanol led to the formation of polydisperse products.<sup>37</sup> As shown in Scheme 1, the Cu precursor CuSO<sub>4</sub>, the protecting ligand 4-mercaptopbenzoic acid (MBA), and NaOH were mixed in a water/ethanol solution (containing 35 vol% ethanol) under stirring condition to form MBA-Cu(I) complexes. Subsequently, a reducing agent (NaBH<sub>4</sub>) was slowly introduced to reduce the MBA-Cu(I) complexes and promote a rapid equilibrium between the forward reduction reaction and the reverse etching reaction,<sup>38</sup> resulting in the formation of yellow atomically-precise Cu<sub>30</sub>(MBA)<sub>16</sub> NCs within 4 h, as illustrated in the inset of Fig. 1a. The synthesized MBA-protected Cu NCs were characterized, and the results revealed an optical absorption peak at 380 nm in the UV-vis absorption spectrum (Fig. 1a). This observation effectively ruled out the production of large-sized Cu nanoparticles (~640 nm) and indicated the formation of monodisperse Cu NCs.<sup>39</sup> Furthermore, the transmission electron microscope (TEM) image revealed a core size of ~1.12 nm for the synthesized Cu NCs, suggesting the formation of ultrasmall Cu NCs (Fig. 1b). The natural polyacrylamide gel electrophoresis (PAGE) analysis of Cu NCs (Fig. 1c) disclosed a single band, demonstrating the excellent monodispersity of the Cu NCs. Notably, size analysis of this type of Cu NCs was conducted with atomic precision in our previous study. Based on the results from electrospray ionization mass spectrometry,<sup>37</sup> their formula was assigned to be Cu<sub>30</sub>(MBA)<sub>16</sub> NCs.

### 2.2 *In vitro* antimicrobial activity and cytotoxicity of Cu<sub>30</sub> NCs

The Cu<sub>30</sub> NCs showed excellent antibacterial activity against both Gram-negative and Gram-positive bacteria. As indicated in Fig. 2a, Cu<sub>30</sub> NCs significantly inhibited the growth of *E. coli* and *S. aureus* in the culture medium compared to the PBS control group. Particularly, Cu NCs with a total concentration of 10 μM (based on Cu ions) exhibited a high antibacterial performance

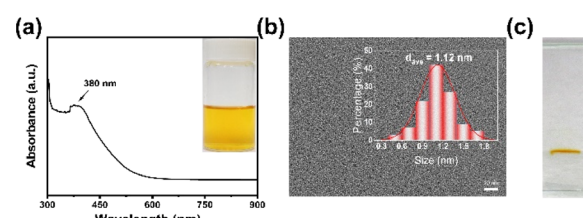


**Fig. 1** Characterization of Cu<sub>30</sub> NCs. (a) UV-vis absorption spectrum of Cu<sub>30</sub> NCs in 35 vol% of ethanol. The inset shows digital photograph of Cu<sub>30</sub> NCs solution. (b) TEM image and size distribution histogram (inset) of Cu<sub>30</sub> NCs. (c) PAGE result of Cu<sub>30</sub> NCs.



against *E. coli* and *S. aureus*, with antibacterial rates of 100% and  $99.17 \pm 1.21\%$ , respectively, as shown in Fig. 2b. In addition, we evaluated the antimicrobial effectiveness of  $\text{Cu}_{30}$  NCs against MRSA and *Candida albicans* (Fig. S1 and S2†). The findings demonstrated that the  $\text{Cu}_{30}$  NCs with 20  $\mu\text{M}$  concentration exhibited a  $97.89 \pm 2.94\%$  antibacterial rate against MRSA and a  $99.81 \pm 1.19\%$  antifungal rate against *Candida albicans* under the same testing conditions. The remarkable antimicrobial efficacy of  $\text{Cu}_{30}$  NCs can be attributed to their ultrasmall size and high surface-to-volume ratio, as well as the inherent antibacterial properties of Cu species. These characteristics significantly enhance atomic utilization and antimicrobial performance. Additionally, the as-designed  $\text{Cu}_{30}$  NCs simultaneously possess ultrasmall size, excellent antibacterial performance, and cost-effectiveness compared to other antibacterial agents (*i.e.*, silver-gallium nano-amalgamated particles and polycationic silver NCs),<sup>12,15</sup> increasing the acceptance in peritonitis treatment.

Upon treatment with  $\text{Cu}_{30}$  NCs, the cell morphology of *E. coli* and *S. aureus* undergoes a noticeable transformation from a plump and smooth appearance (Fig. S3a and S4a†) to an atrophic and wrinkled state (Fig. S3b and S4b†), indicating the disruption of the cell membrane. To gain a deeper insight into the antibacterial mechanism, two experiments were conducted. Initially, the cell uptake behavior of *E. coli* was investigated by measuring the optical absorbance of  $\text{Cu}_{30}$  NCs before and after incubation with *E. coli*. The results in Fig. S5† revealed a significant decrease in the optical absorbance of  $\text{Cu}_{30}$  NCs at 380 nm from 2.94 to 1.67 after the separation of *E. coli* from the  $\text{Cu}_{30}$  NCs solution *via* centrifugation, suggesting that 46.3% of the  $\text{Cu}_{30}$  NCs were absorbed on the membrane of *E. coli* or endocytosed by the bacterium. Subsequently, transmission electron microscope (TEM) analysis was employed to examine the cell uptake behavior of *E. coli* for  $\text{Cu}_{30}$  NCs, with *E. coli* cells incubated with  $\text{Cu}_{30}$  NCs being fixed prior to TEM analysis. Fig. S6† illustrated clear cell morphology with a fractured membrane of *E. coli*, along with numerous ultra-tiny black dots ( $\text{Cu}_{30}$  NCs) observed both on the cell membrane and within the cell. Based on this data, it can be inferred that the absorption and internalization of  $\text{Cu}_{30}$  NCs by *E. coli* may trigger the generation of ROS, leading to oxidative stress, subsequent ROS production, and eventual destruction of the cell membrane, resulting in the inactivation or dysfunction of the bacteria.<sup>31,33</sup> It is worth noting that the peptidoglycan membrane of Gram-negative *E. coli* is thinner compared to Gram-positive *S.*

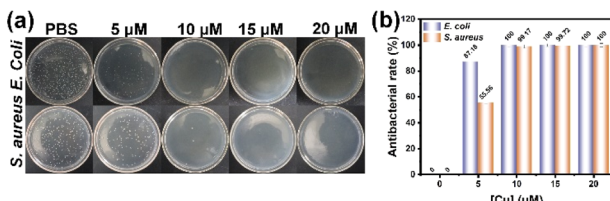


Fig. 2 (a) *In vitro* antibacterial results of  $\text{Cu}_{30}$  NCs with a concentration range of 5–20  $\mu\text{M}$  against *E. coli* and *S. aureus* with the usage of PBS as control. (b) Antibacterial rates of  $\text{Cu}_{30}$  NCs against *E. coli* and *S. aureus*.

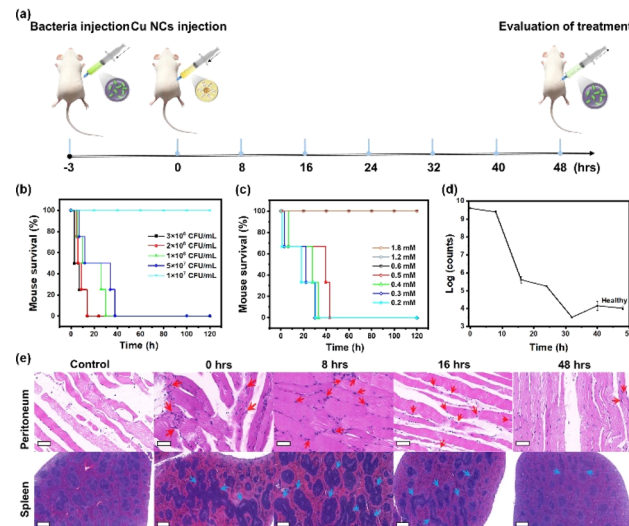


Fig. 3 *In vivo* evaluation of the therapeutic effect of  $\text{Cu}_{30}$  NCs on peritonitis in mice. (a) Schematic illustration for the animal experimentation timeline. (b) Survival rate of mice after injection with different concentrations of *E. coli*. (c) Survival rate of peritonitis mice after injection with different concentrations of  $\text{Cu}_{30}$  NCs. (d) Bacterial quantity within the peritoneal cavity of mice after treatment with  $\text{Cu}_{30}$  NCs for different time. (e) H&E staining of histological sections including spleen and peritoneum of mice with acute peritonitis after treatment with  $\text{Cu}_{30}$  NCs for different time. The increasing inflammatory cells on peritoneum and the enlarged lymphoid nodules on spleen are marked with red and blue arrows, respectively. The normal mice without any infection were used as a control group. Scale bar, 50  $\mu\text{m}$  (peritoneum group), 500  $\mu\text{m}$  (spleen group).

*aureus*,<sup>40</sup> rendering the former more susceptible to inactivation. Therefore, this disparity may contribute to the superior antimicrobial effectiveness of  $\text{Cu}_{30}$  NCs against Gram-negative bacteria in comparison to Gram-positive counterparts.

To assess the biological applications, the cytotoxicity of  $\text{Cu}_{30}$  NCs against 4T1 cells was examined using an MTT assay (Fig. S7†). The results revealed that the cytotoxicity of  $\text{Cu}_{30}$  NCs (12.5  $\mu\text{M}$ ) was low, with the 4T1 cells retaining a viability of 96.12% after 24 h, compared to the positive control (ultrapure water) and significantly higher than the negative control (Tween 20, 6.92% cell viability). These results indicate the good biocompatibility of the  $\text{Cu}_{30}$  NCs.

### 2.3 *In vivo* treatment of primary peritonitis with $\text{Cu}_{30}$ NCs

The  $\text{Cu}_{30}$  NCs have exhibited a promising *in vitro* antimicrobial effect, low cytotoxicity, and good biocompatibility, providing strong justification for further investigation of their potential efficacy for treating *in vivo* peritonitis with antibacterial and anti-inflammatory effects. Initial experiments depicted in Fig. 3a involved the establishment of a mouse model of primary peritonitis through intraperitoneal injection of *E. coli* suspended in saline. Notably, the concentration of *E. coli* required to induce 100% mortality in mice after 2 days was found to be  $5 \times 10^7 \text{ CFU mL}^{-1}$ , as illustrated in Fig. 3b. Consequently, this concentration was utilized in subsequent peritonitis induction experiments. Within 3 h post *E. coli* injection, mice exhibited



symptoms characteristic of primary peritonitis such as depression, moodiness, curling up into a ball, and exclusion of mucus feces. Subsequently, mice afflicted with peritonitis were injected with Cu<sub>30</sub> NCs in 100  $\mu$ L saline with varied concentrations, while a saline group served as a control. Fig. 3c illustrates the outcomes where infected mice faced mortality within 120 h when treated with Cu<sub>30</sub> NCs below 0.5 mM. Conversely, administering Cu<sub>30</sub> NCs at concentrations of  $\geq 0.6$  mM resulted in mice surviving normally at 120 h, indicating that the minimum effective concentration for successful primary peritonitis therapy is 0.6 mM. Interestingly, even with a threefold increase in concentration (1.8 mM), all mice maintained a 100% survival rate, suggesting a wide therapeutic window. This result can be ascribed to the outstanding biocompatibility, low biotoxicity, and effective therapeutic action of Cu<sub>30</sub> NCs. Thereafter, the efficacy of 0.6 mM Cu<sub>30</sub> NCs in treating primary peritonitis was evaluated.

The Cu<sub>30</sub> NCs demonstrated notable effectiveness in treating *in vivo* primary peritonitis infected with *E. coli*. Fig. 3d and S8† illustrated the rapid reduction of *E. coli* in the peritoneal cavity of mice following Cu<sub>30</sub> NCs administration, with a subsequent gradual decrease towards normal levels over time. Significantly, the bacterial counts decrease by more than 5 orders of magnitude at 48 h compared to their initial population, indicating the strong bactericidal properties of Cu<sub>30</sub> NCs within organisms. Further validation of the *in vivo* therapeutic effect of Cu<sub>30</sub> NCs was observed through hematoxylin-eosin (H&E) staining (Fig. 3e and S9†). Compared with the control mice with the injection of saline rather than *E. coli*, the peritonitis model exhibited increased inflammatory cells (marked with red arrows, see upper panel in Fig. 3e and S9†) in the peritoneum post-bacterial infection, as well as enlarged splenic lymph nodes (labelled with blue arrows, see lower panel in Fig. 3e and S9†). Fig. S10† displayed the detailed size information of the inflammatory cells and splenic lymph nodes.<sup>11</sup> Notably, the number of inflammatory cells in the peritoneum of the peritonitis mice group increased, peaked at 8 h from the intraperitoneal injection of Cu<sub>30</sub> NCs, and subsequently decreased to normal levels by 48 h. Similarly, splenic lymph nodes reached maximum extension at 8 h from the intraperitoneal injection of Cu<sub>30</sub> NCs, declining significantly by 24 h and returning to normal levels at 40 h. The conclusion that Cu<sub>30</sub> NCs have anti-inflammatory effects is strengthened by the expression levels of anti-inflammatory factors in mice,<sup>41,42</sup> as depicted in Fig. S11.† Specifically, the expression levels of tumor necrosis factor- $\alpha$  (TNF- $\alpha$ , Fig. S11a†), interleukin-6 (IL-6, Fig. S11b†), and interleukin-1 $\beta$  (IL-1 $\beta$ , Fig. S11c†) in the Cu<sub>30</sub> NCs-treated group gradually decreased to levels within the normal range observed

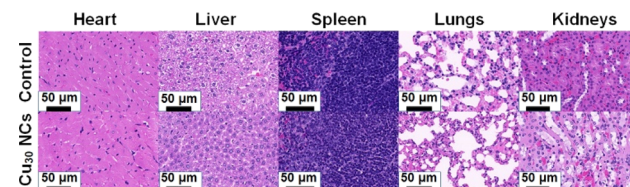


Fig. 4 H&E staining of histological sections including heart, liver, spleen, lungs and kidneys of peritonitis mice 5 days post injection with Cu<sub>30</sub> NCs for *in vivo* biosafety evaluation. The normal mice without any infection were used as a control group.

in uninfected mice. These observations collectively substantiate the remarkable therapeutic effects of Cu NCs against drug-resistant bacterial infections and primary peritonitis. Furthermore, the as-designed Cu<sub>30</sub> NCs showed better therapeutic performance than ampicillin, a commercial antibacterial agent, in peritonitis treatment, which is evidenced by their dose-response curves (Fig. S12†) and *in vivo* antibacterial activities (Fig. S13†), emphasizing the huge potential of Cu<sub>30</sub> NCs in clinical peritonitis treatment.

#### 2.4 *In vivo* biosafety assessment of Cu<sub>30</sub> NCs

The *in vivo* biosafety of Cu<sub>30</sub> NCs is a significant concern, despite the strong confirmation of their superior therapeutic efficacy for primary peritonitis as demonstrated above. To address this concern, H&E staining was carried out on major organs, including the heart, liver, spleen, lungs, and kidneys, in Cu<sub>30</sub> NCs-treated mice five days after the injection of Cu<sub>30</sub> NCs. This was compared with the normal mice as a control, as depicted in Fig. 4. The results revealed that there was no observable histopathological damage or abnormality in the major organs of the mice. Furthermore, blood routine analysis and blood biochemistry tests indicated that all the blood indexes, as well as the liver and kidney functions, were within the normal range (Table 1). These findings clearly showed that Cu<sub>30</sub> NCs are safe and compatible for use in peritonitis therapy, demonstrating their promising potential for *in vivo* application.

The *in vivo* distribution and metabolism of Cu<sub>30</sub> NCs also played a crucial role in biosafety. Fig. 5 revealed that Cu<sub>30</sub> NCs were present in all organs of the mice, with varying quantities. Specifically, initial increments followed by subsequent decreases in Cu<sub>30</sub> NCs levels were observed in the heart, lungs, spleen, and peritoneum within 48 h, indicating non-accumulation in these organs. Conversely, the levels of Cu<sub>30</sub> NCs in the kidneys and liver exhibited an “increase-decrease-increase” pattern within 48 h, signifying a tendency towards

Table 1 Blood routine and liver function parameters for peritonitis mice 5 days post injection with Cu<sub>30</sub> NCs

Name	White blood cell ( $10^9 \text{ L}^{-1}$ )	Monocytes ( $10^9 \text{ L}^{-1}$ )	Neutrophil ( $10^9 \text{ L}^{-1}$ )	Alkaline phosphatase ( $\text{U L}^{-1}$ )	Total protein ( $\text{g L}^{-1}$ )	Alanine aminotransferase ( $\text{U L}^{-1}$ )
Numerical value	2.9	0.2	0.9	157.50	54	34.2
Normal range	0.8–6.8	0.0–0.3	0.1–1.8	62–209	36–66	28–132



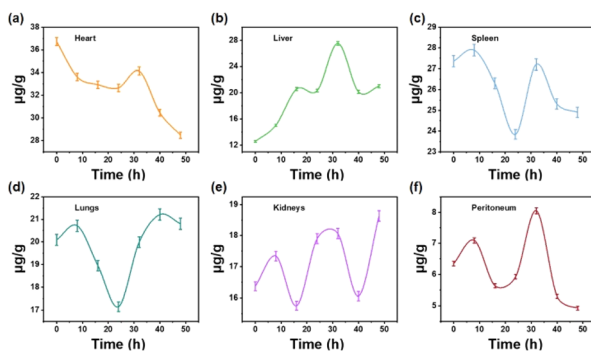


Fig. 5 Time-course biodistribution of Cu<sub>30</sub> NCs in different organs of mice: (a) heart, (b) liver, (c) spleen, (d) lungs, (e) kidneys, and (f) peritoneum.

accumulation. Furthermore, the gradual decrease in Cu<sub>30</sub> NCs content in the heart, lungs, spleen, and peritoneum within 30 h, in conjunction with the increase in the kidneys and liver, provided clear evidence that the clearance of Cu<sub>30</sub> NCs is dependent on the metabolic functions of the liver and kidneys. This observation is consistent with the role of the liver and kidneys as crucial organs for metabolic and detoxification processes in living organisms.

### 3. Conclusions

In summary, water-soluble Cu<sub>30</sub> NCs have been developed as an effective antibacterial agent for treating primary peritonitis. The ultrasmall size of Cu<sub>30</sub> NCs (<1.2 nm) and their excellent antibacterial properties against Gram-negative *E. coli* (100%) have contributed to their remarkable therapeutic effects. Moreover, the treatment with Cu<sub>30</sub> NCs resulted in a reduction of more than 5 orders of magnitude in the number of drug-resistant *E. coli* in the peritoneal cavity of mice with peritonitis and led to the disappearance of pathological features in the peritoneum and spleen. Importantly, no significant toxicities were observed in the group of mice treated with Cu<sub>30</sub> NCs during the tested period, demonstrating their good biocompatibility, low biotoxicity, as well as hepatic and renal clearance. This study is significant in that it sheds light on the design of novel Cu NCs-based antibacterial agents for *in vivo* antibacterial treatment and the elimination of abdominal inflammation.

### Conflicts of interest

The authors declare no conflict of interests.

### Acknowledgements

This work was supported by the National Natural Science Foundation of China (22071127, 22371153, 52301002), the China Postdoctoral Science Foundation (2023M731854), the Taishan Scholar Foundation of Shandong Province (tsqn201812074), the Qingdao Postdoctoral Science Foundation (QDBSH20230101003), and the Youth Innovation Team

Development Program of Shandong Higher Education Institutions (2022KJ155).

### Notes and references

- K. Zheng, M. I. Setyawati, D. T. Leong and J. Xie, *Coord. Chem. Rev.*, 2018, **357**, 1–17.
- F. Jiao, W. Zhao, W. Zhao, Y. Wang, Y. Deng, S. Chang, J. Sun, Q. Lou, L. Wang, C.-X. Shan, Y. Xiao and L. Dong, *BMEMat*, 2023, **1**, e12055.
- B. McCall, L. Shaller, M. Wilson and A. Hayward, *npj Antimicrob. Resist.*, 2023, **1**, 10.
- E. R. Rojas, G. Billings, P. D. Odermatt, G. K. Auer, L. Zhu, A. Miguel, F. Chang, D. B. Weibel, J. A. Theriot and K. C. Huang, *Nature*, 2018, **559**, 617–621.
- R. Laxminarayan, A. Duse, C. Wattal, A. K. M. Zaidi, H. F. L. Wertheim, N. Sumpradit, E. Vlieghe, G. L. Hara, I. M. Gould, H. Goossens, C. Greko, A. D. So, M. Bigdeli, G. Tomson, W. Woodhouse, E. Ombaka, A. Q. Peralta, F. N. Qamar, F. Mir, S. Kariuki, Z. A. Bhutta, A. Coates, R. Bergstrom, G. D. Wright, E. D. Brown and O. Cars, *Lancet Infect. Dis.*, 2013, **13**, 1057–1098.
- R. Ruhal and R. Kataria, *Microbiol. Res.*, 2021, **251**, 126829.
- D. Saxena, R. Maitra, R. Bormon, M. Czekanska, J. Meiers, A. Titz, S. Verma and S. Chopra, *npj Antimicrob. Resist.*, 2023, **1**, 17.
- H. C. Neu, *Science*, 1992, **257**, 1064–1073.
- D. Pörner, S. Von Vietinghoff, J. Nattermann, C. P. Strassburg and P. Lutz, *Expert Opin. Pharmacother.*, 2021, **22**, 1567–1578.
- S. M. Manani, G. M. Virzì, A. Giuliani, M. Baretta, V. Corradi, M. De Cal, C. Biasi, C. Crepaldi and C. Ronco, *Blood Purif.*, 2020, **49**, 434–439.
- Y. Wang, X. Ding, Y. Chen, M. Guo, Y. Zhang, X. Guo and H. Gu, *Biomaterials*, 2016, **101**, 207–216.
- T. T. Nguyen, P. Zhang, J. Bi, N. H. Nguyen, Y. Dang, Z. Xu, H. Wang, N. Ninan, R. Bright, T. Pham, C. K. Nguyen, Y. Sabri, M. T. Nguyen, J. Vongsivut, Y. Zhao, K. Vasilev and V. K. Truong, *Adv. Funct. Mater.*, 2023, **23**, 10539.
- X. Wang, B. Yin, L. Jiang, C. Yang, Y. Liu, G. Zou, S. Chen and M. Zhu, *Science*, 2023, **381**, 784–790.
- Q. Yao, X. Yuan, T. Chen, D. T. Leong and J. Xie, *Adv. Mater.*, 2018, **30**, 1802751.
- E. O. Uroro, R. Bright, P. R. L. Dabare, J. Y. Quek, N. Goswami and K. Vasilev, *Mater. Today Chem.*, 2023, **28**, 101376.
- S. Li, J. Wei, Q. Yao, X. Song, J. Xie and H. Yang, *Chem. Soc. Rev.*, 2023, **52**, 1672–1696.
- W. Zhong, K. Liang, W. Liu and L. Shang, *Chem. Sci.*, 2023, **14**, 8823–8830.
- G. Yang, X. Pan, W. Feng, Q. Yao, F. Jiang, F. Du, X. Zhou, J. Xie and X. Yuan, *ACS Nano*, 2023, **17**, 15605–15614.
- G. Yang, Z. Wang, F. Du, F. Jiang, X. Yuan and J. Y. Ying, *J. Am. Chem. Soc.*, 2023, **145**, 11879–11898.
- X. Zhu, L. Chen, Y. Liu and Z. Tang, *Polyoxometalates*, 2023, **2**, 9140031.
- Q. Yao, L. Liu, S. Malola, M. Ge, H. Xu, Z. Wu, T. Chen, Y. Cao, M. F. Matus, A. Pihlajamäki, Y. Han, H. Häkkinen and J. Xie, *Nat. Chem.*, 2023, **15**, 230–239.



22 S.-S. Zhang, S. Havenridge, C. Zhang, Z. Wang, L. Feng, Z.-Y. Gao, C. M. Aikens, C.-H. Tung and D. Sun, *J. Am. Chem. Soc.*, 2022, **144**, 18305–18314.

23 Y. Zhong, J. Zhang, T. Li, W. Xu, Q. Yao, M. Lu, X. Bai, Z. Wu, J. Xie and Y. Zhang, *Nat. Commun.*, 2023, **14**, 658.

24 X. Kang and M. Z. Zhu, *Chem. Soc. Rev.*, 2019, **48**, 2422–2457.

25 M.-M. Zhang, X.-Y. Dong, Z.-Y. Wang, X.-M. Luo, J.-H. Huang, S.-Q. Zang and T. C. W. Mak, *J. Am. Chem. Soc.*, 2021, **143**, 6048–6053.

26 Y. Zhou, L. Liao, S. Zhuang, Y. Zhao, Z. Gan, W. Gu, J. Li, H. Deng, N. Xia and Z. Wu, *Angew. Chem., Int. Ed.*, 2021, **60**, 8668–8672.

27 X. Jiang, B. Du, Y. Huang and J. Zheng, *Nano Today*, 2018, **21**, 106–125.

28 X. Cai, G. Saranya, K. Shen, M. Chen, R. Si, W. Ding and Y. Zhu, *Angew. Chem., Int. Ed.*, 2019, **58**, 9964–9968.

29 H. Liu, Y. Li, S. Sun, Q. Xin, S. Liu, X. Mu, X. Yuan, K. Chen, H. Wang, K. Varga, W. Mi, J. Yang and X.-D. Zhang, *Nat. Commun.*, 2021, **12**, 114.

30 X.-K. Wan, J.-Q. Wang and Q.-M. Wang, *Angew. Chem., Int. Ed.*, 2021, **60**, 20748–20753.

31 H. Zhu, S. Wang, Y. Wang, C. Song, Q. Yao, X. Yuan and J. Xie, *Biomaterials*, 2022, **288**, 121695.

32 Z. Wang, Y. Fang, X. Zhou, Z. Li, H. Zhu, F. Du, X. Yuan, Q. Yao and J. Xie, *Nano Res.*, 2020, **13**, 203–208.

33 Z. Zuo, X. Pan, G. Yang, Y. Zhang, X. Liu, J. Zha and X. Yuan, *Dalton Trans.*, 2023, **52**, 2942–2947.

34 X. Wang, Z. Wang, S. Fang, Y. Hou, X. Du, Y. Xie, Q. Xue, X. Zhou and X. Yuan, *Chem. Eng. J.*, 2021, **420**, 127589.

35 L. Wang, Q. Hou, W. Zheng and X. Jiang, *ACS Nano*, 2021, **15**, 17885–17894.

36 T. Jia, Z.-J. Guan, C. Zhang, X.-Z. Zhu, Y.-X. Chen, Q. Zhang, Y. Yang and D. Sun, *J. Am. Chem. Soc.*, 2023, **145**, 10355–10363.

37 Y. Ge, X. Yali, W. Yaru, T. Ying, C. L. Leng, J. Fuyi, D. Fanglin, Z. Xianfeng, Y. J. Ying and Y. Xun, *Nano Res.*, 2023, **16**, 1748–1754.

38 X. Yuan, B. Zhang, Z. Luo, Q. Yao, D. T. Leong, N. Yan and J. Xie, *Angew. Chem., Int. Ed.*, 2014, **53**, 4623–4627.

39 Y.-e. Shi, J. Ma, A. Feng, Z. Wang and A. L. Rogach, *Aggregate*, 2021, **2**, e112.

40 X. Yuan, M. I. Setyawati, D. T. Leong and J. Xie, *Nano Res.*, 2014, **7**, 301–307.

41 R. Yan, S. Sun, J. Yang, W. Long, J. Wang, X. Mu, Q. Li, W. Hao, S. Zhang, H. Liu, Y. Gao, L. Ouyang, J. Chen, S. Liu, X.-D. Zhang and D. Ming, *ACS Nano*, 2019, **13**, 11552–11560.

42 J.-M. Cavaillon, *Toxicon*, 2018, **149**, 45–53.

